Theoretical prediction of new C–Si alloys in $C2/m$-20 structure*

Xiangyang Xu(徐向阳), Changchun Chai(柴常春), Qingyang Fan(樊庆扬)†, and Yintang Yang(杨银堂)

State Key Discipline Laboratory of Wide BandGap Semiconductor Technology, School of Microelectronics, Xidian University, Xi'an 710071, *China*

(Received 4 December 2016; revised manuscript received 9 January 2017; published online 20 February 2017)

We study structural, mechanical, and electronic properties of C_{20}, Si_{20} and their alloys ($C_{16}Si_4$, $C_{12}Si_8$, C_8Si_{12}, and C_4Si_{16}) in $C2/m$ structure by using density functional theory (DFT) based on first-principles calculations. The obtained elastic constants and the phonon spectra reveal mechanical and dynamic stability. The calculated formation enthalpy shows that the C–Si alloys might exist at a specified high temperature scale. The ratio of B/G and Poisson's ratio indicate that these C–Si alloys in $C2/m$-20 structure are all brittle. The elastic anisotropic properties derived by bulk modulus and shear modulus show slight anisotropy. In addition, the band structures and density of states are also depicted, which reveal that C_{20}, $C_{16}Si_4$, and Si_{20} are indirect band gap semiconductors, while C_8Si_{12} and C_4Si_{16} are semi-metallic alloys. Notably, a direct band gap semiconductor ($C_{12}Si_8$) is obtained by doping two indirect band gap semiconductors (C_{20} and Si_{20}).

Keywords: C–Si alloys, mechanical properties, band structure, direct band gap semiconductor

PACS: 61.50.–f, 61.50.Ah, 71.20.Nr, 71.55.Cn **DOI:** 10.1088/1674-1056/26/4/046101

1. Introduction

As the first plentiful element on the earth, carbon has kinds of allotropes with a wide range of structures from superhard wide semiconductors to ultra-soft semimetals and even superconductors. The carbon allotropes have been investigated maturely and applied in many fields. The researches show that carbon allotropes own advanced mechanical and electronic properties. Xing *et al.*[1] came up with $C2/m$-20 carbon and compared with two other monoclinic symmetry carbon allotropes ($C2/m$-16 carbon and M-carbon) and found that $C2/m$-20 carbon shows the greatest elastic modulus, anisotropy in Young's modulus and hardness. Moreover, there are many other superhard carbon allotropes that have been predicted by researchers, such as O-carbon,[2] W-carbon,[3] F-carbon,[4] C-carbon,[5] lonsdaleite,[6] Z-carbon,[7] H-carbon,[8] $C_{48(2i+1)}$,[9] S-carbon,[10] *Imma*-carbon,[11] (9, 0)-carbon,[12] and so on. As the cornerstone of high-tech materials, silicon is widely applied in the production of high-purity semiconductors, high temperature materials, and optical fiber communication materials. Fan *et al.*[13] put forwards four novel silicon allotropes (*Amm*2, $C2/m$-16, $C2/m$-20, and I-4); the mechanical and dynamical stability at ambient condition were proved. In addition, $C2/m$-16, $C2/m$-20, and I-4 phases were indirect band gap semiconductors materials with band gap of 0.56, 0.53, and 1.28 eV, respectively. The *Amm*2 phase was a quasi-direct gap phase with a gap of 0.74 eV. The anisotropy properties show that the $C2/m$-20 phase exhibits greater anisotropy in shear elastic anisotropic factors.

C–Si alloys are attracting more and more attention in industry and academia[14–23] because of their potential standout properties different from elemental carbon and silicon. In the converter steelmaking field, C–Si alloys are a new type of converter alloys, which can replace ferrosilicon, silicon carbide, and carburizer, further reducing the amount of deoxidizing agent. They have a good prospect in the process of converter for the stability, hardness, and mechanical properties which is superior to traditional technology. Recently, physicists are proceeding to find new kinds of C–Si alloys with splendid structural, mechanical, and electronic properties. Especially, direct band gap semiconductors are the direction researchers are interested in because it is easy for the energy transition to occur and they are appropriate for optoelectronic devices. Based on the global particle-swarm optimization algorithm and the density functional theory methods, Zhou *et al.*[24] predicted a novel energetically and thermally stable two-dimensional SiC_2 siligraphene (g-SiC_2) which is a semiconductor with a direct band gap of 1.09 eV. From first principles combined with a tight-binding model, Zhao *et al.*[25] proposed siligraphenes g-SiC_3 and g-Si_3C, both of which are dynamically stable and the spin–orbital coupling (SOC) band gaps are 0.431 meV (g-SiC_3) and 0.089 meV (g-Si_3C), much larger than those of graphene (0.0008 meV) and planar silicene (0.07 meV). Yan *et al.*[26] obtained three stable Si_mC_n graphyne-like structures and studied through the structural relaxation, optimization, electronic structures as well as the thermal stability. Beside two-dimensional structures of silicon carbides, there are many works regarding the three-dimensional silicon carbide materials. Zhang *et al.*[27] proposed two new phases of Si_8C_4 and Si_4C_8 with the $P4_2/mnm$ symmetry and studied their structural, elastic, and electronic properties systematically. Both of them are proved to be me-

*Project supported by the National Natural Science Foundation of China (Grant No. 61474089) and the Open Fund of Key Laboratory of Complex Electromagnetic Environment Science and Technology, China Academy of Engineering Physics (Grant No. 2015-0214.XY.K).

†Corresponding author. E-mail: qyfan_xidian@163.com

© 2017 Chinese Physical Society and IOP Publishing Ltd

chanically and dynamically stable. The band gaps of Si_8C_4 and Si_4C_8 are 0.74 eV and 0.15 eV, respectively, and both of them are indirect semiconductors. Fan *et al.*[28] investigated the structural, mechanical, anisotropic, and electronic properties of SiC_2 and SiC_4. The calculated results show that SiC_2 and SiC_4 are anisotropic materials and that SiC_2 is an indirect band gap semiconductor while SiC_4 is a quasi-direct band gap semiconductor. Tan *et al.*[29] proposed C–Si alloys (C_8Si_2, C_6Si_4, C_4Si_6, and C_2Si_8) in the orthorhombic structure of $P222_1$ space group and proved the mechanical stability and elastic anisotropic. The concluded band structure exhibits that the proposed C–Si alloys are all indirect band gap semiconductors.

Based on the previous works, we propose four new structures of C–Si alloys ($C_{16}Si_4$, $C_{12}Si_8$, C_8Si_{12}, and C_4Si_{16}) in $C2/m$ structure. In this paper, the lattice parameters and elastic constants are first calculated using first-principles calculations. Then the elastic modulus, Poisson's ratio, hardness, elastic anisotropy, and Debye temperature are obtained. In addition, the band structures and density of states of C_{20}, Si_{20}, and their alloys are investigated and analyzed.

2. Theoretical method

The structural, mechanical and electronic properties of C_{20}, Si_{20}, and their alloys ($C_{16}Si_4$, $C_{12}Si_8$, C_8Si_{12}, and C_4Si_{16}) in $C2/m$ structure were studied utilizing Cambridge Serial Total Energy Package (CASTEP)[30] based on DFT.[31] The exchange correlation potential was performed with the generalized gradient approximation (GGA) in the form of Perdew–Burke–Ernzerhof (PBE),[32] PBE for solid (PBEsol),[33] and the local density approximation (LDA) in the form of Ceperley and Alder data parameterized by Perdew and Zunger (CA-PZ).[34,35] To describe the core-valence interactions, the ultrasoft pseudo potentials were introduced. The cutoff energy of C_{20} ($C_{16}Si_4$, $C_{12}Si_8$, C_8Si_{12}, and C_4Si_{16}) and Si_{20} was 400 eV and 340 eV, respectively. The valence electron structures of C and Si atoms are $2s^22p^2$ and $3s^23p^2$ and the grid partitions of k-points in the first irreducible Brillouin zone[36] were set as $7\times16\times8$, $7\times16\times8$, $7\times15\times7$, $6\times13\times6$, $5\times13\times6$, and $5\times10\times5$, respectively. For C_{20}, Si_{20}, and four new C–Si alloys phases, the structures were optimized using Broyden–Fletcher–Goldfarb–Shanno (BFGS)[37] minimization algorithm. The convergence tolerance was 5×10^{-6} eV/atom and the SCF (self-consistent field) tolerance was 5×10^{-7} eV/atom. On the atom, the maximum force is 0.01 eV/Å with the maximum stress 0.02 GPa and the maximum displacement 5×10^{-4} Å.

3. Results and discussion

Figure 1 illustrates the crystal structures of C_{20}, Si_{20}, and their alloys ($C_{16}Si_4$, $C_{12}Si_8$, C_8Si_{12}, and C_4Si_{16}). They all belong to the space group of $C2/m$ in a monoclinic system and every conventional cell includes 20 atoms. By utilizing PBE, PBEsol, and CA-PZ methods, the structures were optimized and the calculated lattice parameters (a, b, c, and β) are listed in Table 1 along with the theoretical value. From Table 1, it is clear that the lattice parameters of C_{20}, Si_{20} in $C2/m$ structure are excellently consistent with other theoretical values.[1,13] From C_{20} to C–Si alloys, even to Si_{20}, the lattice parameters (a, b, and c) increase with the number of Si atoms as shown in Fig. 2. Additionally, the curves of the GGA method (PBE and PBEsol) show a little better performance than the one of the LDA method (CA-PZ) in spite of the fact that all the curves in Fig. 2 almost coincide.

As we all know, the elastic constants of a conventional cell are very significant in researching on the mechanical properties of a crystal, which offer information about the stability and stiffness of the materials. For monoclinic symmetry space group of $C2/m$, there are thirteen independent elastic constants C_{ij} (C_{11},C_{22}, C_{33}, C_{44}, C_{55}, C_{66}, C_{12}, C_{13}, C_{15}, C_{23}, C_{25}, C_{35}, and C_{46}). The values of elastic constants which were obtained by introducing a small finite strain to the equilibrium structure are listed in Table 2. The elastic constants of C_{20} and Si_{20} were consistent with theoretical value. A stable monoclinic structure must satisfy the following mechanical stability criteria:[38]

$$C_{ii} > 0 \quad (i = 1,2,\ldots,6), \tag{1}$$

$$C_{11} + C_{22} + C_{33} + 2(C_{12} + C_{13} + C_{23}) > 0, \tag{2}$$

$$\left(C_{33}C_{55} - C_{35}^2\right) > 0, \tag{3}$$

$$\left(C_{44}C_{66} - C_{46}^2\right) > 0, \tag{4}$$

$$(C_{22} + C_{33} - 2C_{23}) > 0, \tag{5}$$

$$[C_{22}(C_{33}C_{55} - C_{35}^2) + 2C_{23}C_{25}C_{35} - C_{23}^2C_{55} - C_{25}^2C_{33}] > 0, \tag{6}$$

$$2[C_{15}C_{25}(C_{33}C_{12} - C_{13}C_{23}) + C_{15}C_{35}(C_{22}C_{13} - C_{12}C_{23}) + C_{25}C_{35}(C_{11}C_{23} - C_{12}C_{13})] - [C_{15}^2(C_{22}C_{33} - C_{23}^2) + C_{25}^2(C_{11}C_{33} - C_{13}^2) + C_{35}^2(C_{11}C_{22} - C_{12}^2)] + C_{55}g > 0, \tag{7}$$

$$g = C_{11}C_{22}C_{33} - C_{11}C_{23}^2 - C_{22}C_{13}^2 - C_{33}C_{12}^2 + 2C_{12}C_{13}C_{23}. \tag{8}$$

After verification, it can be found that all the elastic constants obey the mechanical stability criteria, which indicates that these six crystals are mechanically stable. To confirm the dynamic stability of their alloys in $C2/m$-20 phase ($C_{16}Si_4$, $C_{12}Si_8$, C_8Si_{12}, and C_4Si_{16}), the phonon spectra of $C_{16}Si_4$, $C_{12}Si_8$, C_8Si_{12}, and C_4Si_{16} in $C2/m$-20 phase are displayed in Figs. 3(a), 3(b), 3(c), and 3(d). There is no imaginary frequency along the whole Brillouin zone form Fig. 3, indicating that these alloys are all dynamically stable.

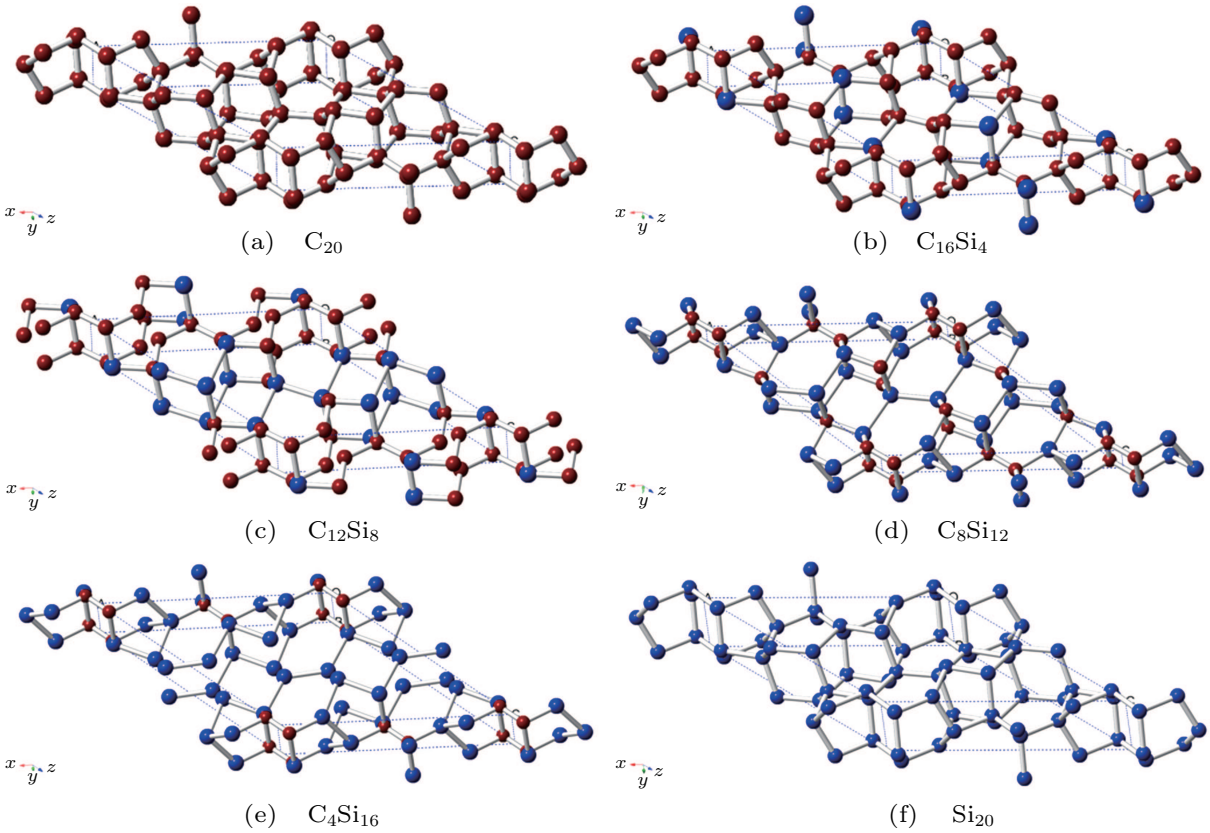


Fig. 1. (color online) Conventional cell crystal structures of C_{20}, Si_{20}, and C–Si alloys (red and blue spheres represent C and Si atoms).

Table 1. Calculated lattice parameters (a, b, c in unit Å and β in unit degree) using PBE, PBEsol, and CA-PZ along with theoretical values.

$C2/m$-20	PBE				PBEsol				CA-PZ			
	a	b	c	β	a	b	c	β	a	b	c	β
C_{20}	9.006	2.519	8.702	143.44	8.979	2.513	8.675	143.39	8.889	2.490	8.597	143.38
C_{20}[a]	9.011	2.519	8.707	143.46								
$C_{16}Si_4$	9.865	2.753	9.546	143.49	9.842	2.742	9.523	143.43	9.736	2.712	9.425	143.49
$C_{12}Si_8$	10.441	3.008	10.474	141.59	10.323	2.999	10.439	141.25	10.233	2.957	10.315	141.36
C_8Si_{12}	11.873	3.140	10.844	142.05	11.894	3.121	10.809	142.02	11.731	3.079	10.671	142.07
C_4Si_{16}	12.355	3.489	11.962	141.37	12.323	3.471	11.923	141.26	12.153	3.421	11.762	141.29
Si_{20}	13.678	3.863	13.232	143.17	13.647	3.857	13.207	143.12	13.443	3.798	13.003	143.11
Si_{20}[b]	13.679	3.863	13.238	143.18								

[a] Ref. [1], [b] Ref. [13].

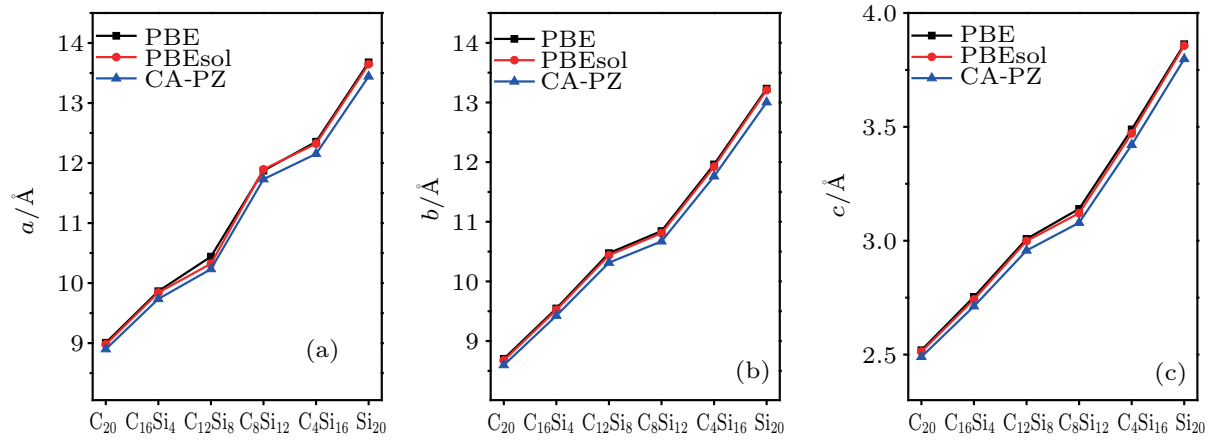


Fig. 2. (color online) Calculated lattice parameters (a, b, and c) of C_{20}, Si_{20}, and C–Si alloys by PBE, PBEsol, and CA-PZ methods.

Table 2. Calculated elastic constants (in unit GPa) and elastic moduli (in unit GPa) of C_{20}, $C_{16}Si_4$, $C_{12}Si_8$, C_8Si_{12}, C_4Si_{16}, and Si_{20}.

	C_{11}	C_{22}	C_{33}	C_{44}	C_{55}	C_{66}	C_{12}	C_{13}	C_{15}	C_{23}	C_{25}	C_{35}	C_{46}
C_{20}	1109	1103	941	455	401	473	45	111	87	39	17	12	59
C_{20}[a]	1105	1249	928	452	398	472	38	108	80	41	16	8	60
$C_{16}Si_4$	672	648	691	271	201	238	64	135	89	–4	20	–9	52
$C_{12}Si_8$	507	457	448	189	173	139	49	69	82	45	47	18	58
C_8Si_{12}	363	276	342	139	101	117	76	68	68	1	4	–35	17
C_4Si_{16}	255	195	219	75	67	49	38	63	47	–1	8	–3	20
Si_{20}	181	167	142	55	45	51	35	44	46	4	6	0	12
Si_{20}[b]	184	167	143	55	52	52	36	46					

[a] Ref. [1], [b] Ref. [13].

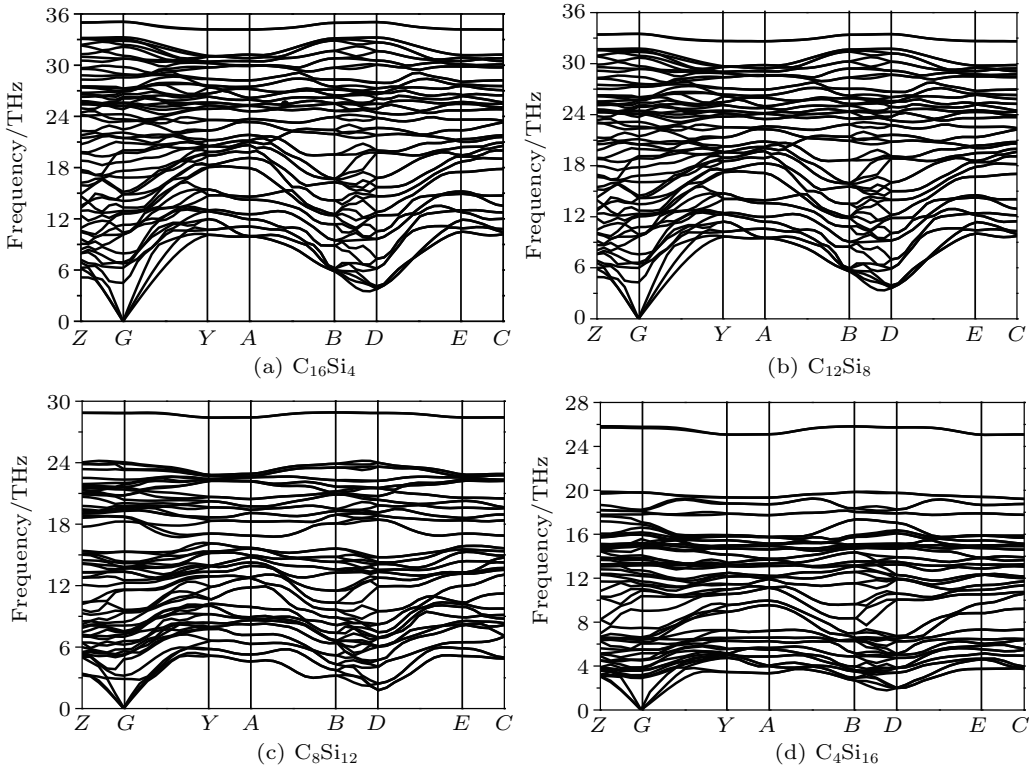


Fig. 3. The phonon spectra of C–Si alloys.

In order to evaluate the relative stability of C–Si alloys, the phase diagram is calculated based on the regular-solution model.[39] The formation energy ΔH of C–Si alloys is defined as follows:

$$\Delta H = E_{\text{total}} - \frac{m}{m+n}E_{\text{C}} - \frac{n}{m+n}E_{\text{Si}}, \tag{9}$$

where E_{total} is the total energy of C–Si alloys, while m and n are the number of C and Si atoms in a conventional cell. The chemical potentials E_{C} and E_{Si} are the total energy of C_{20} and Si_{20}, respectively. The formation energies of C–Si alloys using PBE, PBEsol, and CA-PZ functions are depicted in Fig. 4. The formation energies are all positive, and the alloys might exist at a specified high temperature scale, due to the entropy ΔH effects considered. The Helmholtz free energy ΔG can be expressed as

$$\Delta G = \Delta E - T\Delta H, \tag{10}$$

where ΔE is the internal energy and T is the absolute temperature of the surroundings. Moreover, for the regular solution model of alloys, the entropy ΔH can be given as

$$\Delta H = -R\left[\frac{n}{m+n}\ln\left(\frac{n}{m+n}\right) + \frac{m}{m+n}\ln\left(\frac{m}{m+n}\right)\right], \tag{11}$$

where R represents the gas constant. From Eqs. (10) and (11), it can be seen that the C–Si alloys in $C2/m$ structure can be synthesized in a high temperature environment.

As we all know, the elastic constants C_{11}, C_{22}, and C_{33} character the resistance to linear compression in x, y, and z directions,[40] respectively. The elastic constants C_{44}, C_{55}, and C_{66} are interpreted by the resistances of the crystal with respect to the shear strain at (100), (010), and (001) planes and are regarded as the important parameters relating to the shear modulus. Figure 5(a) shows the elastic constants C_{ii} and it is clear that the calculated C_{11}, C_{22}, and C_{33} are very large

among the thirteen elastic constants, which indicates that they are very incompressible under uniaxial stress along x, y, and z axes. It is easily found that C_{11} is higher than C_{33} for these six crystals except $C_{16}Si_4$. Thus, it can be considered that the z axis is more compressible than the x axis for C_{20}, $C_{12}Si_8$, C_8Si_{12}, C_4Si_{16}, and Si_{20}. In addition, C_{11} is slightly higher than C_{22} for all these six crystals indicating that the y axis is a little more compressible than the x axis. In cases of C_{44}, C_{55}, and C_{66}, for all the studied crystals in this work, C_{44} is larger than C_{55}, so the resistance to the shear strain at the (100) plane is stronger than that of the (010) plane. For $C_{16}Si_4$, $C_{12}Si_8$, C_8Si_{12}, C_4Si_{16}, and Si_{20}, the resistance at (100) is larger than that of the (001) plane. As a whole, with the increasing components of Si atoms, the elastic constants C_{ii} decrease thus the compression property increases.

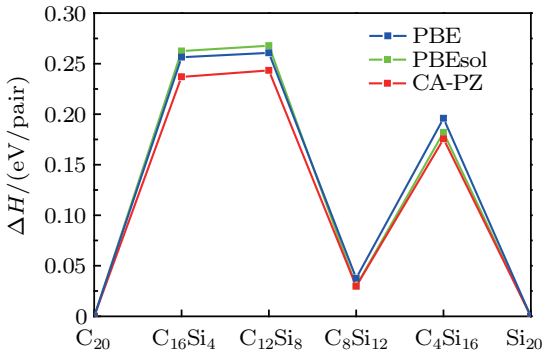


Fig. 4. (color online) The formation energy of C–Si alloys.

Then using the data of Table 2, the elastic moduli can be calculated. To obtain the bulk modulus B (in unit GPa) and the shear modulus G (in unit GPa), which represent the volumetric elasticity and shearing direction under opposing forces, Voigt[41] proposed the upper limits B_V and G_V, while Reuss[42] proposed the lower limits B_R and G_R in the following equations:[43]

$$B_V = (1/9)[C_{11}+C_{22}+C_{33}+2(C_{12}+C_{13}+C_{23})], \quad (12)$$

$$G_V = (1/15)[C_{11}+C_{22}+C_{33}+3(C_{44}+C_{55}+C_{66}) - (C_{12}+C_{13}+C_{23})], \quad (13)$$

$$\begin{aligned} B_R = {} & \Omega[(C_{33}C_{55}-C_{35}^2)(C_{11}+C_{22}-2C_{12}) \\ & +(C_{23}C_{55}-C_{25}C_{35})(2C_{12}-2C_{11}-C_{23}) \\ & +(C_{13}C_{35}-C_{15}C_{33})(C_{15}-2C_{25}) \\ & +(C_{13}C_{55}-C_{15}C_{35})(2C_{12}+2C_{23}-C_{13}-2C_{22}) \\ & +2(C_{13}C_{25}-C_{15}C_{23})(C_{25}-C_{15})+f]^{-1}, \end{aligned} \quad (14)$$

$$\begin{aligned} G_R = {} & 15\{4[(C_{33}C_{55}-C_{35}^2)(C_{11}+C_{22}+C_{12}) \\ & +(C_{23}C_{55}-C_{25}C_{35})(C_{11}-C_{12}-C_{23}) \\ & +(C_{13}C_{35}-C_{15}C_{33})(C_{15}+C_{25}) \\ & +(C_{13}C_{55}-C_{15}C_{35})(C_{22}-C_{12}-C_{23}-C_{13}) \\ & +(C_{13}C_{25}-C_{15}C_{23})(C_{15}-C_{25})+f]/\Omega \\ & +3[(g/\Omega)+(C_{44}+C_{66})/(C_{44}C_{66}-C_{46}^2)]\}^{-1}, \end{aligned} \quad (15)$$

$$f = C_{11}(C_{22}C_{55}-C_{25}^2)-C_{12}(C_{12}C_{55}-C_{15}C_{25}) +C_{15}(C_{12}C_{25}-C_{15}C_{22})+C_{25}(C_{23}C_{35}-C_{25}C_{33}), \quad (16)$$

$$\begin{aligned} \Omega = {} & 2[C_{15}C_{25}(C_{33}C_{12}-C_{13}C_{23})+C_{15}C_{35}(C_{22}C_{13}-C_{12}C_{23}) \\ & +C_{25}C_{35}(C_{11}C_{23}-C_{12}C_{13})]-[C_{15}^2(C_{22}C_{33}-C_{23}^2) \\ & +C_{25}^2(C_{11}C_{33}-C_{13}^2)+C_{35}^2(C_{11}C_{22}-C_{12}^2)] \\ & +(C_{11}C_{22}C_{33}-C_{11}C_{23}^2-C_{22}C_{13}^2-C_{33}C_{12}^2 \\ & +2C_{12}C_{13}C_{23})C_{55}. \end{aligned} \quad (17)$$

However, the arithmetic average of Voigt and Reuss bounds termed as Voigt–Reuss–Hill (VRH)[41–43] approximations is the acknowledged best method to calculate the bulk modulus and the shear modulus. From VRH approximations, we have $B=(B_V+B_R)/2$ and $G=(G_V+G_R)/2$. The Young modulus E is the ratio of stress to strain and can be obtained by $E=9BG/(3B+G)$.[43] Universally, the larger the Young's modulus E is, the stiffer the material is prone to be. Poisson's ratio $v=(3B--2G)/[2(3B+G)]$[43] is the ratio of the expansion fraction to compression fraction.

Aforementioned elastic moduli, i.e., bulk modulus B (in unit GPa), shear modulus G (in unit GPa), Young's modulus E (in unit GPa), and Poisson's ratio v were calculated and shown in Table 3. It is found that the bulk modulus B, the shear modulus G, and the Young modulus E all decrease by 79.72%, 88.31%, and 86.78% with the increase of the Si atoms, meaning that the stiffness decreases. Besides, the slopes of the B, G, and E curves turn smaller and smaller. For the C–Si alloys, the variation tendency of the bulk modulus B and the shear modulus G are almost the same. For the elastic moduli and Poisson's ratio, the given data of this work are consistent with theoretical values. The ratio of the bulk modulus to the shear modulus (B/G) proposed by Pugh[44] indicates the ductile or brittle feature of a material. If $B/G>1.75$, the material manifests the ductile feature, otherwise, the brittle feature. The crystal with Poisson's ratio v larger than 0.26 belongs to ductile material. From Table 3, we can see that B/G for C_{20}, Si_{20} and their alloys ($C_{16}Si_4$, $C_{12}Si_8$, C_8Si_{12} and C_4Si_{16}) is less than 1.75 and Poisson's ratio v is less than 0.26, it is concluded that they are all brittle crystals.

Table 3. Calculated elastic moduli (in unit GPa) and Poisson's ratio v of C_{20}, Si_{20}, $C_{16}Si_4$, $C_{12}Si_8$, C_8Si_{12}, and C_4Si_{16}.

	B/GPa	G/GPa	B/G	E/GPa	v
C_{20}	403	456	0.884	993	0.089
C_{20}[a]	412	463	0.890	1010	0.091
$C_{16}Si_4$	287	252	1.139	585	0.160
$C_{12}Si_8$	198	173	1.144	401	0.161
C_8Si_{12}	155	120	1.292	286	0.192
C_4Si_{16}	106	69	1.536	171	0.232
Si_{20}	82	53	1.547	131	0.232
Si_{20}[b]	83	55	1.509	135	0.230

[a] Ref. [1], [b] Ref. [13].

The hardness of material can express the elastic and plas-

tic properties as follows:

$$H_{\mathrm{V}} = 2(G^3/B^2)^{0.585} - 3. \tag{18}$$

The calculated hardness of C_{20}, $C_{16}Si_4$, $C_{12}Si_8$, C_8Si_{12}, C_4Si_{16}, and Si_{20} are 80, 41, 32, 21, 11, and 9 GPa, respectively, with a tendency of nonlinear decrease. The hardness values of C_{20} and $C_{16}Si_4$ are larger than 40 GPa, thus they are superhard materials while $C_{12}Si_8$ and C_8Si_{12} are hard materials.

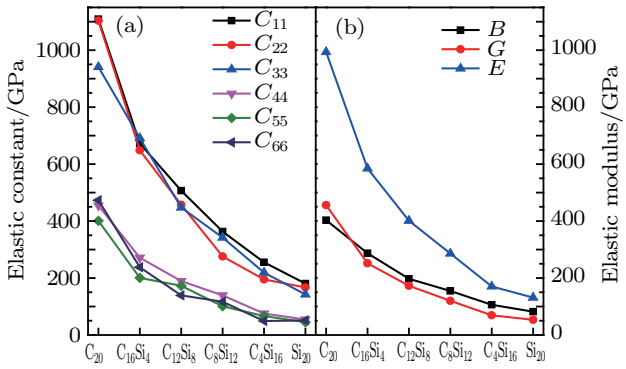


Fig. 5. (color online) Elastic constants C_{ii} and elastic moduli (B, G, and E) of C_{20}, $C_{16}Si_4$, $C_{12}Si_8$, C_8Si_{12}, C_4Si_{16}, and Si_{20}.

The elastic anisotropy is another crucial parameter which relates to the probability of inducing micro-cracks in materials. There are many descriptions of anisotropy named the compression anisotropy A_{B} and the shear anisotropy A_{G} which represent the percentage of the bulk modulus and shear modulus, respectively, and the universal anisotropy index A^{U} can be obtained anisotropy as follows:[45]

$$A_{\mathrm{B}} = \frac{B_{\mathrm{V}} - B_{\mathrm{R}}}{B_{\mathrm{V}} + B_{\mathrm{R}}}, \tag{19}$$

$$A_{\mathrm{G}} = \frac{G_{\mathrm{V}} - G_{\mathrm{R}}}{G_{\mathrm{V}} + G_{\mathrm{R}}}, \tag{20}$$

$$A^{\mathrm{U}} = 5\frac{G_{\mathrm{V}}}{G_{\mathrm{R}}} + \frac{B_{\mathrm{V}}}{B_{\mathrm{R}}} - 6. \tag{21}$$

From the three anisotropy formulas, it is obvious that A_{B}, A_{G}, and A^{U} are all not less than zero. If A_{B}, A_{G}, and A^{U} are equal to zero, the anisotropy eliminates and the crystal turns to isotropic material. If A_{B} and A_{G} equal to 1, then the anisotropy is maximum. From Table 4 and Fig. 6(a), it is easy to be observed that these six studied crystals show weak anisotropy since the values of A_{B} and A_{G} are very small. Meanwhile, the column of A_{B} is a little smaller than the A_{G} column indicating that the anisotropy is inconspicuous in bulk modulus. As shown in Ref. [13], for silicon allotropes, the value of A^{U} in $C2/m$ structure is larger than that of $Amm2$, $C2/m$-16, and I-4 structures, which indicates that the anisotropy of Si_{20} in $C2/m$ structure is greatest. In our work, the values of A^{U} of C_4Si_{16} and $C_{12}Si_8$ are 0.594 and 0.540, respectively, larger than Si_{20} (0.241), so C_4Si_{16} and $C_{12}Si_8$ own stronger universal anisotropy.

Table 4. Compression and shear anisotropy percent factors (A_{B} and A_{G}), universal anisotropy index (A^{U}) and shear anisotropy factors (A_1, A_2, and $A_{3)}$.

	B_{V}	B_{R}	G_{V}	G_{R}	A_{B}	A_{G}	A^{U}	A_1	A_2	A_3
C_{20}	404.2	401.9	459.8	452.2	0.284	0.831	0.090	0.995	0.857	0.891
$C_{16}Si_4$	287.6	287.0	256.9	246.9	0.113	1.984	0.207	0.994	0.692	0.798
$C_{12}Si_8$	201.3	193.3	181.0	164.6	2.014	4.755	0.540	0.928	0.933	0.643
C_8Si_{12}	156.1	153.3	122.6	117.5	0.892	2.122	0.235	0.977	0.839	0.961
C_4Si_{16}	107.2	105.3	73.0	65.5	0.889	5.449	0.594	0.866	0.831	0.526
Si_{20}	82.0	81.4	54.5	52.1	0.382	2.279	0.241	0.925	0.825	0.739
Si_{20}[a]	83.2	82.6	56.3	54.2	0.347	1.971	0.208			

[a] Ref. [13].

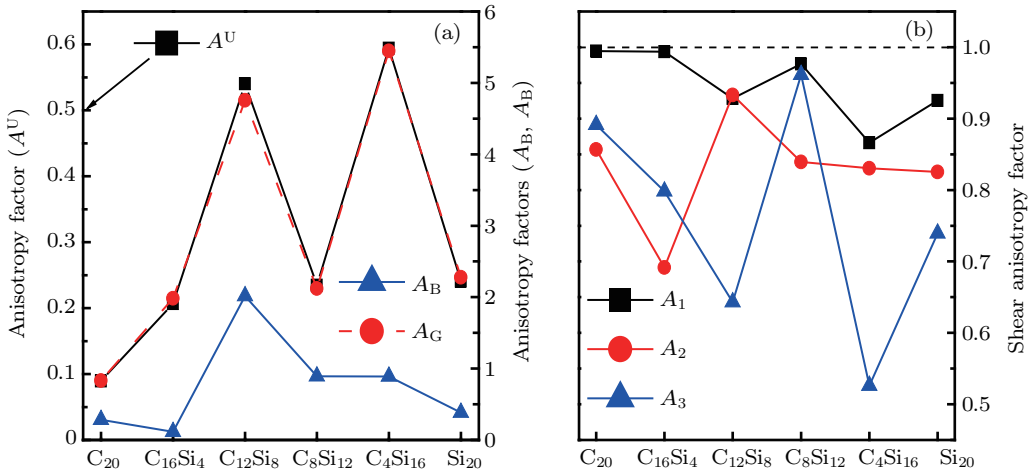


Fig. 6. (color online) Calculated elastic anisotropy factors (a), shear anisotropy factors (b) of C_{20}, $C_{16}Si_4$, $C_{12}Si_8$, C_8Si_{12}, C_4Si_{16}, and Si_{20}.

The shear anisotropic factors provide a measure of the degree of anisotropy in the bonding between atoms in different planes. The shear elastic anisotropic factors A_1, A_2, and A_3 can be defined as:[46]

$$A_1 = \frac{4C_{44}}{C_{11}+C_{33}-2C_{13}}, \tag{22}$$

$$A_2 = \frac{4C_{55}}{C_{22}+C_{33}-2C_{23}}, \tag{23}$$

$$A_3 = \frac{4C_{66}}{C_{11}+C_{22}-2C_{12}}, \tag{24}$$

where A_1 describes the (100) shear plane between [011] and [010] directions, A_2 describes the (010) shear plane between [101] and [001] directions, and A_3 describes the (001) shear plane between [100] and [010] directions, respectively. Table 4 gives the values of the shear anisotropy factors (A_1, A_2, A_3) and figure 6(b) describes the gaps between the factors and horizontal line of 1. If A_1, A_2, and A_3 are equal to one, the crystal belongs to isotropic material. Otherwise, the larger the gap is, the stronger anisotropy the shear plane shows. Observing Fig. 6(b), for C_{20} and $C_{16}Si_4$, the shear planes of (010) and (001) show more anisotropy; for $C_{12}Si_8$, the shear planes of (100) and (010) behave with the same anisotropic character while the (001) plane has the more obvious anisotropy; C_8Si_{12} behaves with the similar small anisotropic character in different directions; for C_4Si_{16} and Si_{20}, they have anisotropy in these three planes. At the shear plane of (100), C_{20}, Si_{20}, and their alloys show weaker shear anisotropy than the other two planes. At the (010) plane, $C_{16}Si_4$ has the strongest shear anisotropy and at the (001) plane $C_{12}Si_8$ and C_4Si_{16} have stronger shear anisotropy.

As a fundamental parameter for evaluating the chemical bonding characteristics and the thermal properties of materials, the Debye temperature Θ_D is generally used to distinguish whether a crystal locates at the high temperature zone or low temperature zone. If the temperature $T > \Theta_D$, the energy is k_BT satisfying the Dulong-Petit law, otherwise, all the modes of high frequency lose efficacy. Combining the electronic structures and the elastic moduli, the Debye temperature can be expressed by the following equations:[47,48]

$$\Theta_D = \frac{h}{k_B}\left[\frac{3n}{4\pi}\left(\frac{N_A\rho}{M}\right)\right]^{1/3} v_m, \tag{25}$$

$$v_m = \left[\frac{1}{3}\left(\frac{2}{v_s^3}+\frac{1}{v_p^3}\right)\right]^{-1/3}, \tag{26}$$

$$v_s = \sqrt{\frac{G}{\rho}}, \quad v_p = \sqrt{\left(B+\frac{4}{3}G\right)\frac{1}{\rho}}, \tag{27}$$

where h is the Planck's constant, k_B is Boltzmann's constant, N_A is the Avogadro's constant, n is the number of atoms in the molecule, M is the molecular weight, ρ is the density of crystal, v_m is the average sound velocity, v_p and v_s represent the compressional and shear sound velocities, respectively. The calculated sound velocities and Debye temperature are listed in Table 5. In general, the melting temperature and the Debye temperature are decided by the interatomic bonding, the bonds between C atoms are larger than those of Si atoms, so the Debye temperature gets lower with the increase of the Si atoms, just as Table 5 shows. The order of the Debye temperature Θ_D in Table 5 is C_{20} >$C_{16}Si_4$ >$C_{12}Si_8$ >C_8Si_{12} >C_4Si_{16} >Si_{20}, consistent with the order of the bulk modulus, shear modulus and Young's modulus.

Table 5. Density (ρ in units g/cm^3), compressional, shear, and average elastic sound velocities (v_p, v_s, v_m in units m/s) as well as Debye temperature (Θ_D in unit K).

	ρ/g·cm^{-3}	v_s/m·s^{-1}	v_p/m·s^{-1}	v_m/m·s^{-1}	Θ_D/K
C_{20}	3.392	11595	17264	12663	2086
$C_{16}Si_4$	3.278	8765	13783	9637	1451
$C_{12}Si_8$	2.996	7594	11948	8350	1145
C_8Si_{12}	2.893	6442	10432	7106	913
C_4Si_{16}	2.566	5194	8796	5755	678
Si_{20}	2.226	4894	8286	5422	585
Si_{20}[a]	2.225	4972	8382	5506	595

[a]Ref. [13].

The electronic band structure describes the law of the electronic motion in a solid and determines the fundamental physical and chemical properties of materials. As is well known, in calculating the band gap, the density functional theory method underestimates the results by 30%–50% compared to the true band gap. The calculated band gaps of C_{20}, Si_{20}, $C_{16}Si_4$, $C_{12}Si_8$, C_8Si_{12}, and C_4Si_{16} are listed in Table 6 by PBE, PBEsol, and CA-PZ methods. The band structure-based PBE are illustrated in Fig. 7 with the dashed line of zero energy representing the Fermi level (E_F). The band gap generally refers to the energy difference between the valence band maximum (VBM) and the conduction band minimum (CBM). The minimal-energy state in the conduction band and the maximal-energy state in the valence band are each characterized by a certain crystal momentum (k-vector) in the Brillouin zone. From Fig. 7, it is obvious to obtain that C_{20}, $C_{16}Si_4$, and Si_{20} are all indirect band gap semiconductors with band widths of 4.02 eV, 0.33 eV, and 0.53 eV, respectively, while $C_{12}Si_8$ is a direct band gap semiconductor with band width of 0.17 eV. The remaining C_8Si_{12} and C_4Si_{16} are semi-metallic alloys. Notably, a direct band gap semiconductor ($C_{12}Si_8$) is obtained by doping two indirect band gap semiconductors (C_{20} and Si_{20}). Meaningfully, $C_{12}Si_8$ is very appropriate for making optoelectronic devices.

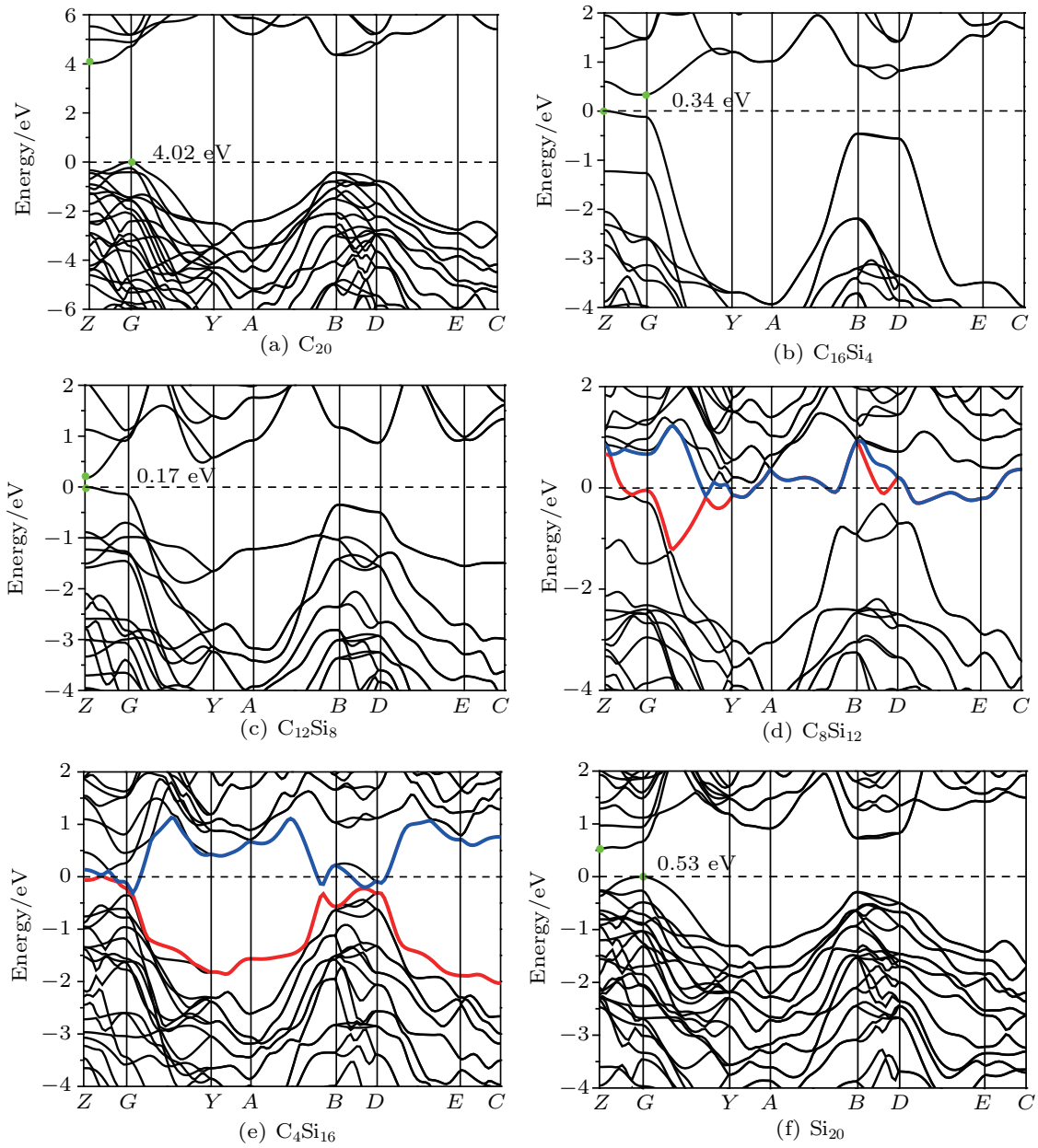


Fig. 7. (color online) Electronic band structures of C_{20}, Si_{20}, and C–Si alloys.

Table 6. The calculated band gap (in unit eV) of C_{20}, $C_{16}Si_4$, $C_{12}Si_8$, C_8Si_{12}, C_4Si_{16}, and Si_{20}.

	C_{20}	C_{20}[a]	$C_{16}Si_4$	$C_{12}Si_8$	C_8Si_{12}	C_4Si_{16}	Si_{20}	Si_{20}[b]
PBE	4.02	4.04	0.33	0.17	–	–	0.53	0.53
PBEsol	3.91		0.13	0.01	–	–	0.40	
CA-PZ	4.08		0.22	0.04	–	–	0.41	

[a] Ref. [1], [b]Ref. [13].

For illustrating the fundamental features of the chemical bonding in $C2/m$, the partial density of states (PDOS) were calculated as shown in Fig. 8. For C_{20}, C-s states make a main contribution in the energy from −22.5 eV to −12.5 eV while C-p states contribute mainly in energy from −12.5 eV to E_F and 4.02 eV to 10 eV. For $C_{16}Si_4$, C-s states make a main contribution in energy from −22 eV to −13 eV and C-p states contribute mainly in energy from −13 eV to E_F and 0.33 eV to 5.5 eV. In addition, Si_5-p contributes mainly in energy from 0.33 eV to 5.5 eV. For $C_{12}Si_8$, C-s states make a main contribution in energy from −18 eV to 11 eV while C-p states contribute mainly in energy from −11 eV to E_F and 0.17 eV to 5.2 eV. It is also found that Si_1-p and Si_5-p contribute mainly in energy from 0.17 eV to 5.2 eV. For C_8Si_{12}, C-s states make a main contribution in energy from −17.5 eV to −10.5 eV while C-p states contribute mainly in energy from −10.5 eV to 3.2 eV. For C_4Si_{16}, C-s states make a main contribution in energy from −16 eV to −8.5 eV while C-p states contribute mainly in energy from −8.5 eV to 3.1 eV. Besides, C4-s contributes mainly in energy from −16 eV to −14 eV. For Si_{20}, Si-s states make a main contribution in energy from −12 eV to −6 eV while Si-p states contribute mainly in energy from −6 eV to E_F and 0.53 eV to 3.35 eV.

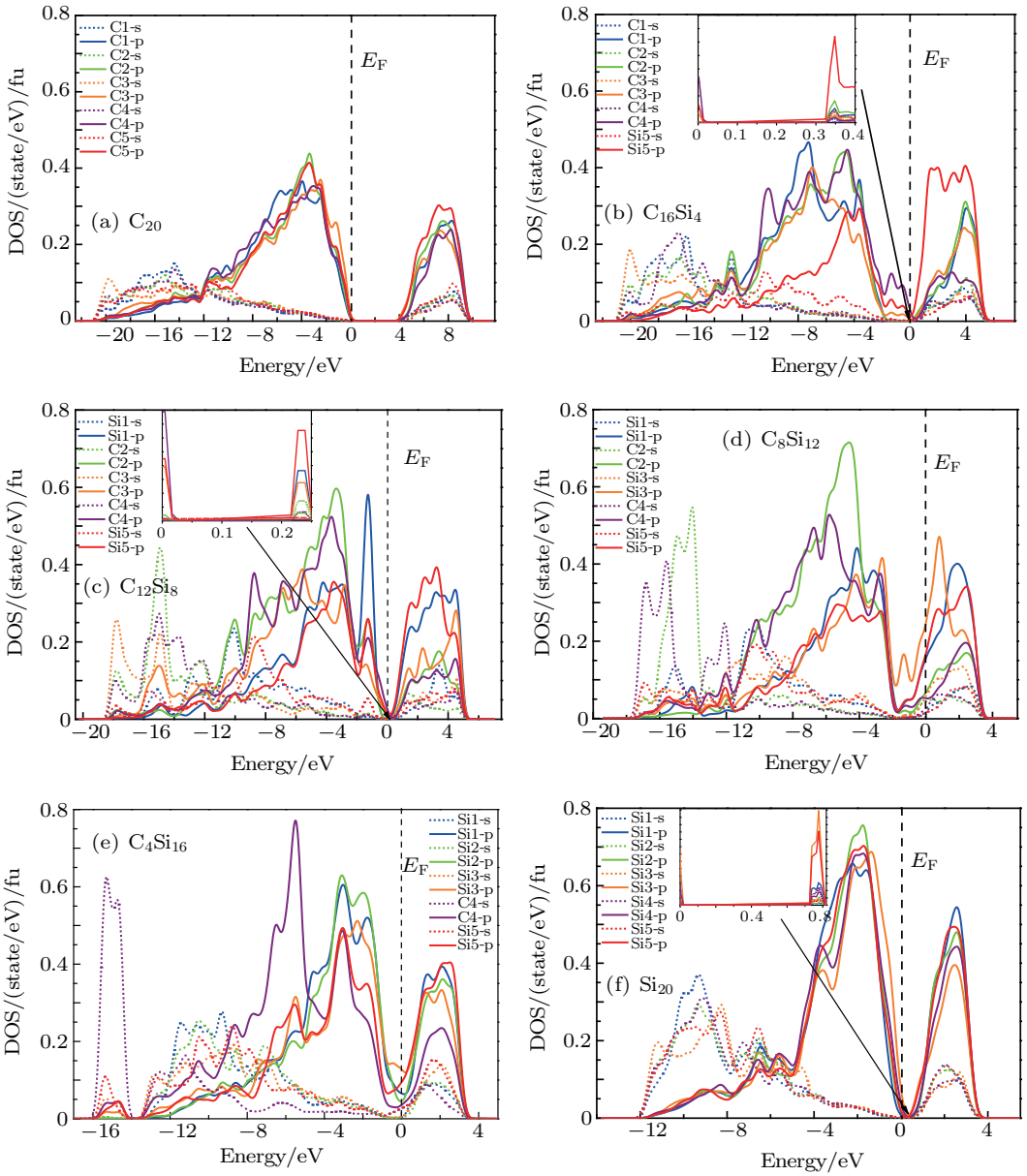


Fig. 8. (color online) Partial densities of states of C_{20}, Si_{20}, and C–Si alloys.

4. Conclusion and perspectives

In this work, the structural properties, elastic properties, anisotropies, and electronic properties of $C_{16}Si_4$, $C_{12}Si_8$, C_8Si_{12}, and C_4Si_{16} in $C2/m$ structure are investigated. The mechanical stability and the dynamic stability are confirmed by the elastic constants and phonon spectra, respectively. It can be found that the B/G and Poisson's ratio all decrease with the increment of the Si atoms, which indicates that they are all brittle crystals. Through the analysis of the compression anisotropy, shear anisotropy, and universal anisotropy factors, C–Si alloys perform a smaller anisotropy. By calculating the band structures, the results show that $C_{16}Si_4$ is indirect band gap semiconductor while $C_{12}Si_8$ is a direct band gap semiconductor, C_8Si_{12} and C_4Si_{16} are semi-metallic alloys. Notably, a direct band gap semiconductor ($C_{12}Si_8$) is obtained by doping two indirect band gap semiconductors (C_{20} and Si_{20}).

References

[1] Xing M J, Li B H, Yu Z T and Chen Q 2015 *Commun. Theor. Phys.* **64** 237
[2] Wang J T, Chen C F and Kawazoe Y 2012 *Phys. Rev. B* **85** 033410
[3] Wang J T, Chen C F and Kawazoe Y 2011 *Phys. Rev. Lett.* **106** 075501
[4] Tian F, Dong X, Zhao Z S, He J L and Wang H T 2012 *J. Phys.: Condens. Matter* **24** 165504
[5] Li D, Bao K, Tian F B, Zeng Z W, He Z, Liu B B and Cui T 2012 *Phys. Chem. Chem. Phys.* **14** 4347
[6] Li Q K, Sun Y, Li Z Y and Zhou Y 2011 *Scr. Mater.* **65** 229
[7] Zhou R L and Zeng X C 2012 *J. Am. Chem. Soc.* **134** 7530
[8] He C Y, Sun L Z, Zhang C X, Peng X Y, Zhang K W and Zhong J X 2012 *Solid State Commun.* **152** 1560
[9] Xu N, Li J F, Huang B L and Wang B L 2016 *Chin. Phys. B* **25** 016103
[10] Sheng X L, Yan Q B, Ye F, Zheng Q R and Su G 2011 *Phys. Rev. Lett.* **106** 155703
[11] Wei Q, Zhang M G, Yan H Y, Lin Z Z and Zhu X M 2014 *Europhys. Lett.* **107** 27007

[12] Xu N, Li J F, Huang B L and Wang B L 2015 *Chin. Phys. B* **24** 066102
[13] Fan Q Y, Chai C C, Wei Q, Yan H Y, Zhao Y B, Yang Y T, Yu X H, Liu Y, Xing M J, Zhang J Q and Yao R H 2015 *J. Appl. Phys.* **118** 185704
[14] Nakashima S and Harima H 1997 *Phys. Stat. Sol.* **39** 162
[15] Walter C and Oestreich M 2008 *Angew. Chem. Int. Ed.* **47** 3818
[16] Han J C, Hu P, Zhang X H, Meng S H and Han W B 2008 *Compos. Sci. Technol.* **68** 799
[17] Zimmermann J, Hilmas G and Fahrenholtz W 2008 *Mater. Chem. Phys.* **112** 140
[18] Gasch M, Ellerby D, Irby E, Beckman S, Gusman M and Johnson S 2004 *J. Mater. Sci.* **39** 5925
[19] Zhu S, Fahrenholtz W and Hilmas G 2007 *J. Eur. Ceram. Soc.* **27** 2077
[20] Dou S X, Soltanian S, Horvat J, Wang X L, Zhou S H, Ionescu M and Liu H K 2002 *Appl. Phys. Lett.* **81** 3419
[21] Guo S, Yang J, Tanaka H and Kagawa Y 2008 *Compos. Sci. Technol.* **68** 3033
[22] Lomello F, Bonnefont G, Leconte Y, Herlin-Boime N and Fantozzi G 2012 *J. Eur. Ceram. Soc.* **32** 633
[23] Wang R Z, Li W G, Li D Y and Fang D N 2015 *J. Eur. Ceram. Soc.* **35** 2957
[24] Zhao M W and Zhang R Q 2014 *Phys. Rev. B* **89** 195427
[25] Zhou L J, Zhang Y F and Wu L M 2013 *Nano Lett.* **13** 5431
[26] Yan X, Xin Z H, Tian L J and Yu M 2015 *Comput. Mater. Sci.* **107** 8
[27] Zhang Q, Wei Q, Yan H Y, Fan Q Y, Zhu X M, Zhang J Q and Zhang D Y 2016 *Z. Naturforsch., A: Phys. Sci.* **71** 387
[28] Fan Q Y, Chai C C, Wei Q and Yang Y T 2016 *Materials* **9** 333
[29] Tan L, Chai C C, Fan Q Y and Yang Y T 2016 *Chin. J. Phys.* **54** 700
[30] Clark S J, Segall M D, Pickard C J, Hasnip P J, Probert M I J, Refson K and Payne M C 2005 *Z. Kristallogr.* **220** 567
[31] Hohenberg P and Kohn W 1964 *Phys. Rev.* **136** B864
[32] Perdew J P, Burke K and Ernzerhof M 1996 *Phys. Rev. Lett.* **77** 3865
[33] Perdew J P, Ruzsinszky A, Csonka G I, Vydrov O A, Scuseria G E, Constantin L A, Zhou X and Burke K 2008 *Phys. Rev. Lett.* **100** 136406
[34] Ceperley D M and Alder B J 1980 *Phys. Rev. Lett.* **45** 566
[35] Perdew J P and Zunger A 1981 *Phys. Rev. B* **23** 5048
[36] Moukhorst J and Pack J D 1996 *Phys. Rev. B* **54** 16533
[37] Pfrommer B G, Côté M, Louie S G and Cohen M L 1997 *J. Comput. Phys.* **131** 233
[38] Wu Z J, Zhao E J, Xiang H P, Hao X F, Liu X J and Meng J 2007 *Phys. Rev. B* **76** 054115
[39] Swalin R A 1962 *Thermodynamics of Solids* (New York: Wiley) p. 243
[40] Hao X P and Cui H L 2014 *J. Korean Phys. Soc.* **65** 45
[41] Voigt W 1928 *Lehrburch der Kristallphysik* (Leipzig: Teubner) p. 739
[42] Reuss A 1929 *Z. Angew. Math. Mech.* **9** 49
[43] Hill R 1952 *Proc. Phys. Soc. London* **65** 349
[44] Pugh S F 1954 *Philos. Mag.* **45** 823
[45] Fan Q Y, Wei Q, Yan H Y, Zhang M G, Zhang Z X, Zhang J Q and Zhang D Y 2014 *Comput. Mater. Sci.* **85** 80
[46] Connétable D and Thomas O 2009 *Phys. Rev. B* **79** 094101
[47] Anderson O L 1963 *J. Phys. Chem. Solids* **24** 909
[48] Panda K B and Ravi K S 2006 *Comput. Mater. Sci.* **35** 134